Influence of the electronic asymmetry in NH ($^1\Delta$) state Λ doublets on the photodissociation dynamics of HN_3 and DN_3

Karl-Heinz Gericke, Michael Lock, Renate Fasold, and Franz Josef Comes
Institut für Physikalische und Theoretische Chemie, Universität Frankfurt (Main), Niederurseler Hang, D-6000 Frankfurt am Main 50, Germany

(Received 26 August 1991; accepted 26 September 1991)

The influence of the electronic asymmetry in the $^1\Delta(A')$ and $^1\Delta(A'')$ Λ doublets of NR (R = H,D) on the photodissociation dynamics of hydrazoic acid (R N_3) has been investigated. Hydrazoic acid was prepared in its first excited electronic state, $\tilde{A}\,^1A''$. A variety of scalar (internal state and translational energy distribution) and vectorial (angular distribution, rotational alignment, correlation between translational and rotational motion) properties of the ejected NH or ND fragment were analyzed by Λ-doublet-specific Doppler profile measurements. While the population of the $^1\Delta(A')$ and $^1\Delta(A'')$ states are equal, the vector correlations for both Λ sublevels are different. N$R(A'')$ products are preferentially ejected in the original plane formed by the parent, and the recoil of NR fragments in the symmetric $\Delta(A')$ state is preferentially perpendicular to that plane. The vector correlation between the translational and the rotational motion of the fragment also indicates a strong nonplanar dissociation geometry for NR products in the $\Delta(A')$ state. About 50% of the ND(A') product rotation is generated by a torsional motion, while 80% of the ND(A'') fragments are formed with **J** being aligned perpendicular to the recoil direction ($M_J = 0$).

I. INTRODUCTION

Polarized laser beams are an excellent tool to determine vector correlations in anisotropic processes. One laser beam selects parent molecules with the proper alignment, while the probe beam analyzes the degree of alignment of the products using different detection geometries and rotational branches for fragment excitation. An analysis is possible not only of the rotational motion **J** of the fragment relative to its recoil velocity **v** or relative to the transition dipole moment **μ** of the parent molecule, but also of the spatial distribution of the products relative to the transition dipole moment.[1-4]

If the diatomic fragments are formed in open-shell electronic states, then the product distribution among the fine-structure levels may provide considerable information on the dynamics of the chemical process. In linear molecules with a nonvanishing projection of the electronic orbital angular momentum onto the nuclear axis, each rotational level is split into closely spaced Λ doublets. At high angular momentum **J**, these two levels have opposite symmetry, $\Lambda(A')$ or $\Lambda(A'')$, with respect to the reflection in the plane of rotation.[5-7] In principle, the relative populations of the $\Lambda(A')$ and $\Lambda(A'')$ doublets can be predicted by projection of a transition state onto the products, if the geometry of the process is conserved.[8,9] Specific Λ doublet preferences were observed in a number of product molecules in Π electronic states formed in reactions[10-25] and photodissociation processes,[26-38] as OH$(X\,^2\Pi)$,[2,13-21,26-33] NO$(X\,^2\Pi)$,[22,23,34-36] and NH$(c\,^1\Pi)$.[37,38] A planar transition state correlates with either one or with the other product Λ state at high rotation, depending on symmetry. These arguments also hold for fragments formed in Δ electronic states.[39-41]

In an infrared multiphoton dissociation experiment of hydrazoic acid, a distinct preference for the production of NH $(a\,^1\Delta)$ fragments in the symmetric $\Delta(A')$ level was observed.[42,43] Since the wave function of the parent HN_3 $(\tilde{X}\,^1A')$ and the wave function of the N_2 $(X\,^1\Sigma_g^+)$ product are symmetric with respect to reflection at the molecular plane, the wave function of the NH $(a\,^1\Delta)$ product must also be symmetric with respect to reflection at the initial molecular plane of the parent, if the HN_3 remains planar during fragmentation. Consequently, the preferred production of NH in the symmetric $\Delta(A')$ state is consistent with a planar dissociation geometry.

On the contrary, in the UV photodissociation of HN_3 at 266 nm,

$$HN_3(\tilde{X}\,^1A') + h\nu(266\ \text{nm}) \rightarrow HN_3(\tilde{A}\,^1A'') \rightarrow NH(a\,^1\Delta) + N_2(X\,^1\Sigma_g^+),$$

no Λ doublet preference was found.[39] Thus, the excited-state dissociation dynamics are governed by nonplanar fragmentation geometries.[44]

In the present study we want to report on a new feature of the $\Delta(A')$ and $\Delta(A'')$ Λ levels in the UV photodissociation of HN_3 and its deuterated analogon DN_3 at 308 nm. There is no preference for one Λ state, i.e., the population of these levels is equal. However, the vector correlations between **μ**(R N_3), **v**(NR), and **J**(NR) behave differently for the two Λ doublets; R = H,D.[45] In addition, the complete product state distribution of the ND$(a\,^1\Delta, v'' = 0)$ fragment is determined.

II. EXPERIMENT

The experiments were performed using the pump and probe technique including sub-Doppler laser-induced flu-

 0021-9606/92/010422-11$06.00

orescence measurements of nascent $NR(a\,^1\Delta)$ products. Details of the experimental setup have been published elsewhere.[39,44] In short, hydrazoic acid was generated in a vacuum line using NaN_3 in excess of (deuterated) stearic acid. The only gases evolving at 75–85 °C were DN_3 and HN_3 which were pumped directly into the observation cell. Typical pressures were 0.5–2.0 Pa controlled by a capacitance manometer.

The photolysis pulse at 308 nm (4.0 eV) was delivered by an XeCl excimer laser (Lambda Physik, EMG 101) operating at a repetition rate of 10 Hz. The pulse energy inside of the observation cell was about 1 mJ at a beam diameter of 2–4 mm. The NH and ND products were probed after a delay time of less than 40 ns by a Nd:YAG pumped dye laser (Lambda Physik, FL 2002E) whose bandwidth was reduced to $\Delta\nu_l \approx 0.1\ \mathrm{cm}^{-1}$ by an intracavity etalon. The bandwidth of this laser system is sufficient to discriminate between NH and ND rotational lines and to resolve the shape of the $(c\,^1\Pi \leftarrow a\,^1\Delta)$ rotational transitions of the (0, 0) band in order to analyze the $(\boldsymbol{\mu} - \mathbf{v} - \mathbf{J})$ vector correlations. The pulse energies of both laser beams were monitored by two Si detectors and stored in a microcomputer (Siemens AT 386) after analog-to-digital conversion.

For measurements of the vector correlations both laser beams were linearly polarized. The plane of polarization of the dye laser was rotated by $\lambda/2$ plates. The polarization plane of the photolysis laser beam was modulated by a photoelastic modulator (Hinds International, PEM 80) on a shot-to-shot basis switching the electric **E** vector between being parallel and being perpendicular to the direction of the analyzing dye laser beam. This laser-beam arrangement allowed experiments at four different probe geometries where the photoelastic modulator switches between geometry II and V and between geometry IV and VI.[2]

The laser-induced fluorescence signal was viewed perpendicular to the laser beams with a photomultiplier tube (Valvo) equipped with $f1.0$ imaging optics and an interference filter (327 ± 5 nm corresponding to the $c\,^1\Pi \rightarrow a\,^1\Delta$ emission). The photomultiplier output was fed to a boxcar integrator (Stanford, SRS 250) which was interfaced to the microcomputer. All time events in the experiments were controlled by a home built three channel variable delay unit which synchronized the photolysis laser with the photoelastic modulator and the dye laser system.

III. RESULTS

The correlated vector properties of a molecular photofragment provide a pictorial view of the dissociation process and, hence, of the upper potential energy surface(PES). Here, the analyzed vectors are the transition dipole moment $\boldsymbol{\mu}$ of the $R\,N_3$ parent, the $NR(a\,^1\Delta)$ product recoil velocity **v**, and the N*R* rotational motion **J**. This dynamical information can be extracted from the shape of the N*R* absorption lines.[2] If the fragments are formed with a single recoil velocity $v = \Delta\nu_D c/\nu_0$, then the Doppler profile $I(x_D)$ of the nonisotropic recoil distribution induced by a linearly polarized photolysis laser is given by

$$I(x_D) \sim \frac{1}{\Delta\nu_D}\left[1 + \beta_{\mathrm{eff}} P_2(x_D)\right], \tag{1}$$

where $x_D = (\nu - \nu_0)/\Delta\nu_D$ is the relative Doppler shift from line center ν_0 and $P_2(x_D)$ is the second Legendre polynomial. The parameter β_{eff} contains all the information about the anisotropy of the dissociation process.[1,2]

Expression (1) has to be convoluted with the line shape of the analyzing dye laser (linewidth $\Delta\nu_l$), the translational motion of the $R\,N_3$ parent at room temperature T $[\Delta\nu_p = \nu_0/c \cdot (8kT \ln 2/m)^{1/2}]$, and with the recoil velocity distribution $f(v)$. If the velocity distribution $f(v)/v$ of the fragment is small or can be approximated by a Gaussian function centered around a mean velocity with a width of $\Delta\nu_f$, then a least-squares fit to the observed Doppler profile yields the anisotropy parameter β_{eff}, the mean Doppler width $\Delta\nu_D$, and the width $\Delta\nu_f$ of the recoil velocity distribution of the fragment:

$$\Delta\nu_f^2 = \Delta\nu_a^2 - \Delta\nu_l^2 - \Delta\nu_p^2. \tag{2}$$

We have measured the values of β_{eff} for NH and ND as a function of the rotational state for each Λ doublet at four different geometries and for all *P*, *Q*, and *R* branches. The bipolar moments $(\beta_{\mu v}, \beta_{vJ}, \beta_{\mu J}, \beta_{\mu vJ})$ which quantitatively describe the vector correlation between the transition dipole moment of the parent $\boldsymbol{\mu}$, the recoil velocity **v**, and the rotational vector **J** of the NH (or ND) product have been determined for each rotational state in the usual manner described in the literature.[2,39] The rotational alignment and the rotational product distribution $P(J)$ of the fragments were determined by the integrated line intensities

$$\int I(\nu_a)\,d\nu_a \sim P(J) \cdot (b_0 + b_1 \beta_{\mu J}), \tag{3}$$

where the geometry and branch dependent multipliers b_0 and b_1 were calculated for observation of undispersed fluorescence.[39]

A. Population of the Λ doublets

In the analysis of N*R* products, the two electron $^1\Delta$ state is excited to a $^1\Pi$ state. In that case, each rotational transition consists of a pair of lines[39] where one line probes the symmetric $\Delta(A')$ state and the adjacent line analyzes the antisymmetric $\Delta(A'')$ state. The energy splitting between the Λ doublets is much larger in the Π state than in the Δ state and, thus, the separation between the line pairs is essentially determined by the (upper) $c\,^1\Pi$ state. At low product rotation, the Doppler width of the lines is larger than the spacing between a line pair. A plot of the population ratios of resolved lines, $R = [P(A'') - P(A')]/[P(A'') + P(A')]$, is shown in Fig. 1. An exclusive formation of N*R* in the antisymmetric $\Delta(A'')$ corresponds to $R = +1$, while the other extreme is obtained for $R = -1$. An unequal population of the two Λ doublet states contains information on the planarity of the fragmentation process. However, within the small range of 10% no strong preference for a Λ doublet level is observed.

Only for ND a minor positive *R* value indicates a slight-

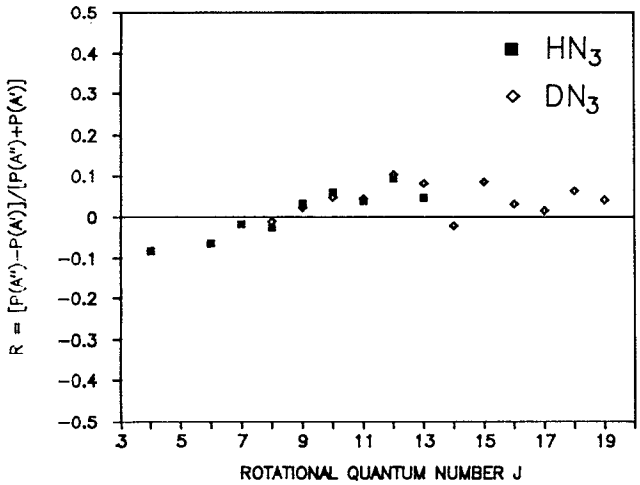

FIG. 1. Relative population ratio of the $^1\Delta(A')$ and $^1\Delta(A'')$ Λ doublets as a function of NH (squares) and ND (rhombi) rotation. A strong positive value of $R = [P(A'') - P(A')]/P[(A'') + P(A')]$ indicates a preferred formation of NH products in the antisymmetric $^1\Delta(A'')$ state which is expected for a planar dissociation process.

ly preferred formation of ND products in the $\Delta(A'')$ state. The photodissociation of jet-cooled HN_3 at 248 nm yielded the same result.[44] In principle, the transition probabilities for the line pair may be different which would suggest different populations for the Λ level. However, a scan at a higher pressure of 130 Pa of the precursor molecule and longer delay times (2 μs) yielded equal populations for both Λ states.

B. Rotational state distribution

The rotational product state distribution of $NR(a\,^1\Delta, v = 0)$ in the photodissociation of hydrazoic acid at 308 nm is shown in Fig. 2. Since no significantly preferred population of a Λ sublevel is observed, the product state distribution is given as the average of the $^1\Delta(A')$ and $^1\Delta(A'')$ state populations. The squares in Fig. 2 represent the NH fragment and the rhombi its deuterated analog. The solid line represents a Gaussian fit to the population number:

$$P(J) = P_0 \cdot \exp\left[-4 \ln 2 \left(\frac{J - J_{\max}}{\Delta J} \right)^2 \right], \tag{4}$$

where $J_{\max}$ is the most likely product rotation and ΔJ represents the full width at half maximum (FWHM) of the rotational distribution. Obviously, the product rotation can well be characterized by a Gaussian distribution. However, it should be mentioned that the unusual behavior at $J_{ND} = 10$ is reproducible in the experiment. The most likely NR rotation $J_{\max}$ is almost doubled, when the H atom is substituted by deuterium; the fit yields $J_{\max}(ND) \approx 10.5$ and $J_{\max}(NH) \approx 5.7$. The width ΔJ also increases from $\Delta J(NH) \approx 5$ to $\Delta J(ND) \approx 9$.

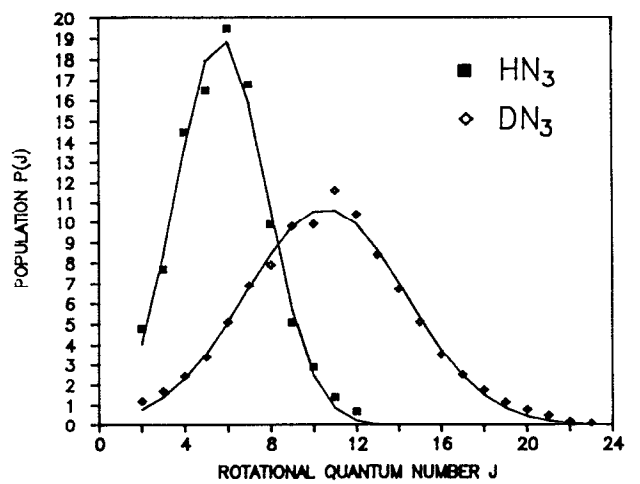

FIG. 2. Rotational state distribution of NH (squares) and ND (rhombi) products generated in the photodissociation of HN_3 and DN_3 at 308 nm. The solid lines are Gaussian functions which are obtained by a least-squares-fit procedure.

C. Energetics

The available energy for the products, E_a, is given by $E_a = h\nu + E_{\text{int}}(R\,N_3) - E_{\text{diss}}$. The internal energy E_{int} is essentially determined by parent rotation $\frac{3}{2}RT$, and to a minor extent, by the $\nu_5(a')$ (NNN) in-plane and by the $\nu_6(a'')$ NNN out-of-plane bend; $E_{\text{int}}(HN_3) \approx 380\ \text{cm}^{-1}$ and $E_{\text{int}}(DN_3) \approx 390\ \text{cm}^{-1}$. The energy E_{diss} is a critical quantity, because a precise value of the bond dissociation energy for generating fragments in their lowest quantum state is not known. However, Casassa *et al.*[43] showed that the most likely value for the fragmentation of $HN_3(\tilde{X}\,^1A')$ into $N_2(^1\Sigma_g^+)$ and $NH(^1\Delta)$ is close to $E_{\text{diss}}(HN_3) \approx 18\,750\ \text{cm}^{-1}$. From this value we calculated the dissociation energy for DN_3 simply by the zero-point vibrational energy difference of HN_3-DN_3 and NH-ND according to the values in Table I. Then we obtain a value of $E_{\text{diss}}(DN_3) \approx 18\,970\ \text{cm}^{-1}$ and for the available energy $E_a(NH) \approx 14\,100\ \text{cm}^{-1}$ and $E_a(ND) \approx 13\,890\ \text{cm}^{-1}$. The mean rotational energy of the ND fragment in $v = 0$ is calculated in the usual manner:

$$\langle E_{\text{rot}} \rangle = \sum_J P(J) E_{\text{rot}}(J) = 1175\ \text{cm}^{-1},$$
$$f_{\text{rot}} = \langle E_{\text{rot}} \rangle / E_a = 0.08. \tag{5}$$

From the line profile measurements we obtain the width $\Delta\nu_D$ and, thus, the recoil velocity of the fragment, $v = \Delta\nu_D \cdot c/\nu_0$. On the average, the ND fragments are formed with a velocity of $\langle v \rangle = 3100$ m/s. Since the linear momentum of ND and N_2 have to compensate each other due to conservation of linear momentum, the mean kinetic energy of the fragments is given by

$$\langle E_{\text{kin}} \rangle = \tfrac{1}{2} m_{\text{ND}}^2 \langle v_{\text{ND}}^2 \rangle / \mu = 10\,100\ \text{cm}^{-1},$$
$$f_{\text{kin}} = \langle E_{\text{kin}} \rangle / E_a = 0.73, \tag{6}$$

where μ is the reduced mass of the ND-N_2 system. The fraction of the available energy which is released as translation is

TABLE I. Normal modes and frequecies of HN_3 (Ref. 49) and DN_3 (Ref. 56) and the population of vibrational excited levels at 300 K. The internuclear distances and angles are essentially the same for both species, except for the ND bond distance being 0.3 pm shorter.

Mode	Vibration	ω/cm^{-1}		$P(v>0)/\%$	
		HN_3	DN_3	HN_3	DN_3
$\nu_1(a')$	*R*-N stretch	3336	2480	0.0	0.0
$\nu_2(a')$	asym. N-N-N	2140	2141	0.0	0.0
$\nu_3(a')$	sym. N-N-N	1274	1183	0.2	0.2
$\nu_4(a')$	*R*-N-N bend	1150	958	0.4	0.9
$\nu_5(a')$	N-N-N in plane	522	496	7.8	8.6
$\nu_6(a'')$	N-N-N out-of-plane	672	587	3.6	5.4
Distance	r(NNN-*R*)/pm	101.5	101.2		

$$\langle E_{\text{kin}}(\text{ND})\rangle = \frac{\mu}{m_{\text{ND}}}\langle E_{\text{kin}}\rangle = 6430\ \text{cm}^{-1},$$
$$\langle E_{\text{kin}}(\text{N}_2)\rangle = \frac{\mu}{m_{\text{N}_2}}\langle E_{\text{kin}}\rangle = 3670\ \text{cm}^{-1}. \tag{7}$$

Since the total energy has to be conserved, we obtain for the mean internal energy of the N_2 partner product:

$$\langle E_{\text{int}}(\text{N}_2)\rangle = E_a - \langle E_{\text{int}}(\text{ND})\rangle - \langle E_{\text{kin}}\rangle = 2580\ \text{cm}^{-1},$$
$$f_{\text{int}}(\text{N}_2) = 1 - f_{\text{rot}}(\text{ND}) - f_{\text{kin}} = 0.19. \tag{8}$$

D. Vector correlations of $\Delta(A')$ and $\Delta(A'')$ Λ doublets

The vector correlation between the transition dipole moment of RN_3, $\mu(\tilde{A}\,^1A'' - \tilde{X}\,^1A')$, and the rotational vector **J** of the N*R* product is described by the value of $\beta_{\mu J}$, which is the normalized rotational alignment parameter $A_0^{(2)} = \frac{4}{5}\beta_{\mu J}$. The limiting values of $\beta_{\mu J} = +1$ or $\beta_{\mu J} = -0.5$ correspond to a parallel or a perpendicular alignment between μ and **J**. We determined $\beta_{\mu J}$ for both Λ sublevels by measuring the integrated line intensities for different excitation branches and detection geometries. Within the experimental uncertainty of $\pm$ 10% no different alignment of the **J** vector relative to the parent transition dipole moment was observed. Figure 3 shows the rotational dependence of the (Λ averaged) $\beta_{\mu J}$ parameter. Only at low *J* a small positive $\beta_{\mu J}$ parameter is observed. In general, the fragmentation process does not prefer an alignment between $\mu(RN_3)$ and **J**(N*R*).

The system behaves completely differently regarding the other vector correlations; i.e., correlations between the transition dipole moment $\mu(RN_3)$ and the fragment recoil velocity **v**(N*R*) and between the translational, **v**(N*R*), and rotational, **J**(N*R*), motion of the product. These correlations can be extracted from the line shapes. It is most surprising that the Λ doublets $\Delta(A')$ and $\Delta(A'')$ indicate different vector correlations. As an example, the Doppler profiles for the $R(9)$ transitions of the NH product are shown in Fig. 4. The line at lower excitation energies probes the antisymmetric $\Delta(A'')$ level, while the adjacent line analyzes the symmetric $\Delta(A')$ state.

Figures 5–7 show the parameters $\beta_{\mu v}$, β_{vJ}, and $\beta_{\mu vJ}$ depicting the vector correlations as a function of product rotation. The open squares and rhombi represent the $\Delta(A')$ state, while the other Λ component, $\Delta(A'')$, is characterized by a solid square. Although the Λ doublets show different

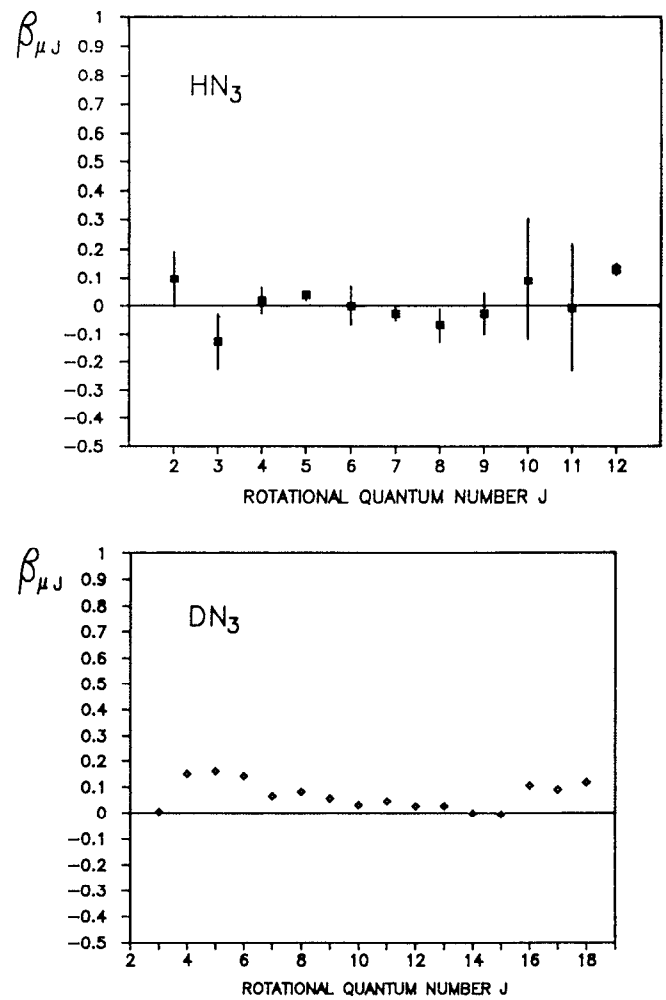

FIG. 3. Rotational alignment $\beta_{\mu J}$ of NH (squares) and ND (rhombi) products. The value of $\beta_{\mu J} \approx 0$ indicates a statistical alignment of the rotational vector **J** relative to the transition dipole moment μ of the parent.

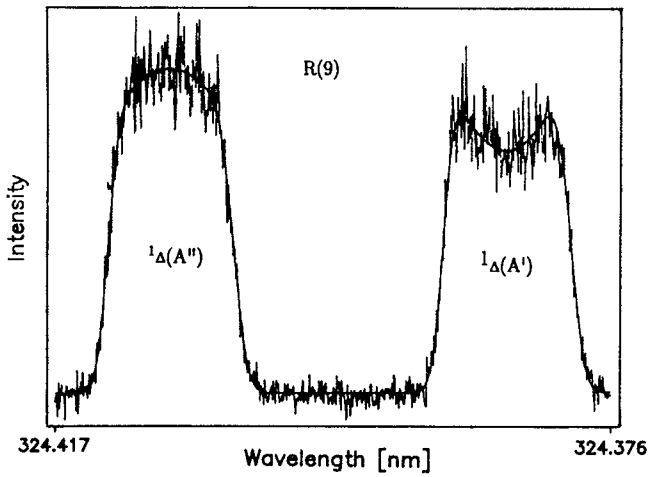

FIG. 4. Line profiles of the $R(9)$ transition of NH formed in the photodissociation of HN_3 at 308 nm. Both lines probe the same rotational state, $J = 9$, but different Λ components.

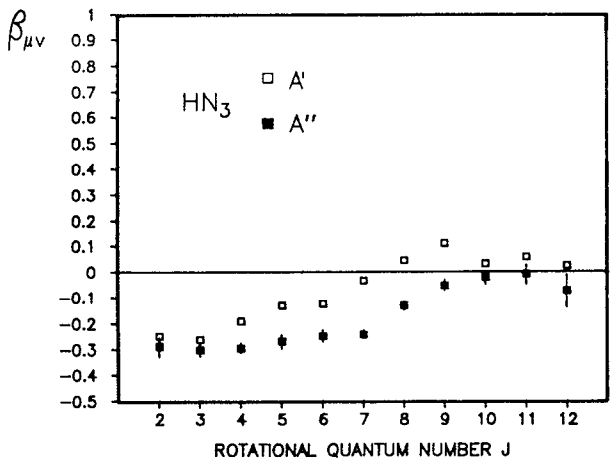

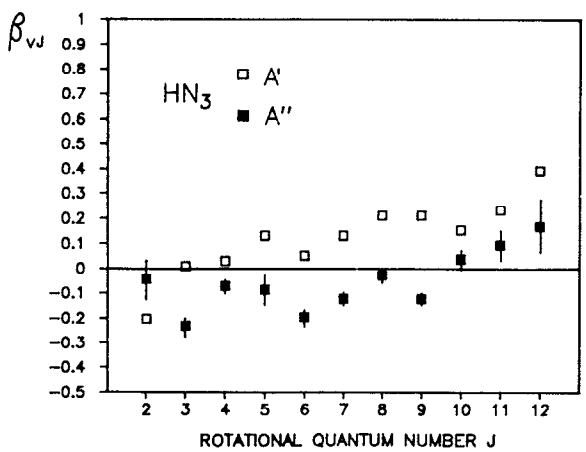

FIG. 5. NH vector correlation between the transition dipole moment μ of the parent HN_3 and the recoil velocity v (upper panel) and between the translational and rotational motion of the product (lower panel). The open squares represent the symmetric $^1\Delta(A')$ state and the solid squares the antisymmetric $^1\Delta(A'')$ state.

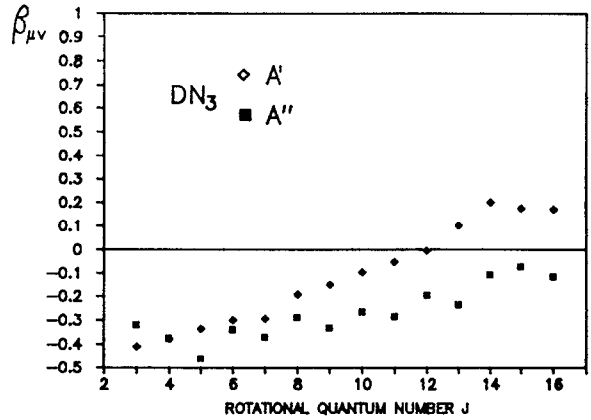

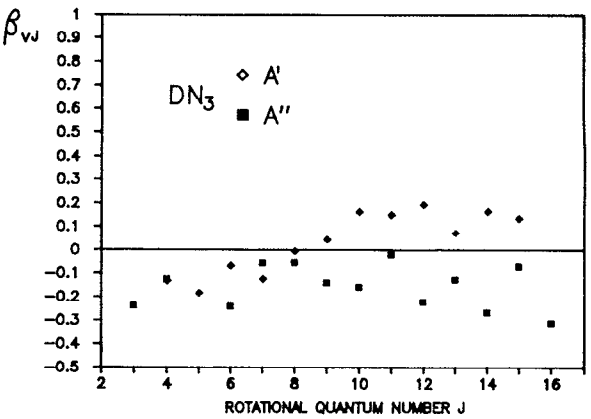

FIG. 6. Vector correlations for the ND product. Same representation as in Fig. 5. The open rhombi represent the symmetric $^1\Delta(A')$ state and the solid squares the antisymmetric $^1\Delta(A'')$ state.

vector correlations, the general trend is the same in terms of the J dependence. The spatial anisotropy of the photoproducts is described by $\beta_{\mu v}$ which is proportional to the classical anisotropy parameter $\beta = 2\beta_{\mu v}$.[1] For low fragment rotation, $\beta_{\mu v}$ is negative indicating a preference for a perpendicular alignment between μ and v [Figs. 5(a) and 6(a)]. With increasing product rotation the value of $\beta_{\mu v}$ increases and finally becomes even positive for the symmetric $\Lambda(A')$ component, showing a slight preference for a parallel alignment between μ and v. However, the $\beta_{\mu v}$ value of the antisymmetric $\Lambda(A'')$ component of the ND fragment remains still negative and, thus, indicates a different spatial distribution of these fragments.

Figures 5(b) and 6(b) show the correlation between the translational and the rotational motion of the NH [Fig. 5(b)] and ND [Fig. 6(b)] product in the photodissociation of $R\,N_3$ at 308 nm. In both cases we observe an increasing $\langle \mathbf{v}\cdot\mathbf{J} \rangle$ correlation with increasing NR rotation for the symmetric $\Delta(A')$ state. Since a positive β_{vJ} parameter indicates a preferentially parallel alignment between $\mathbf{v}$ and $\mathbf{J}$, this rotational NR motion can only be generated by an out-of-plane

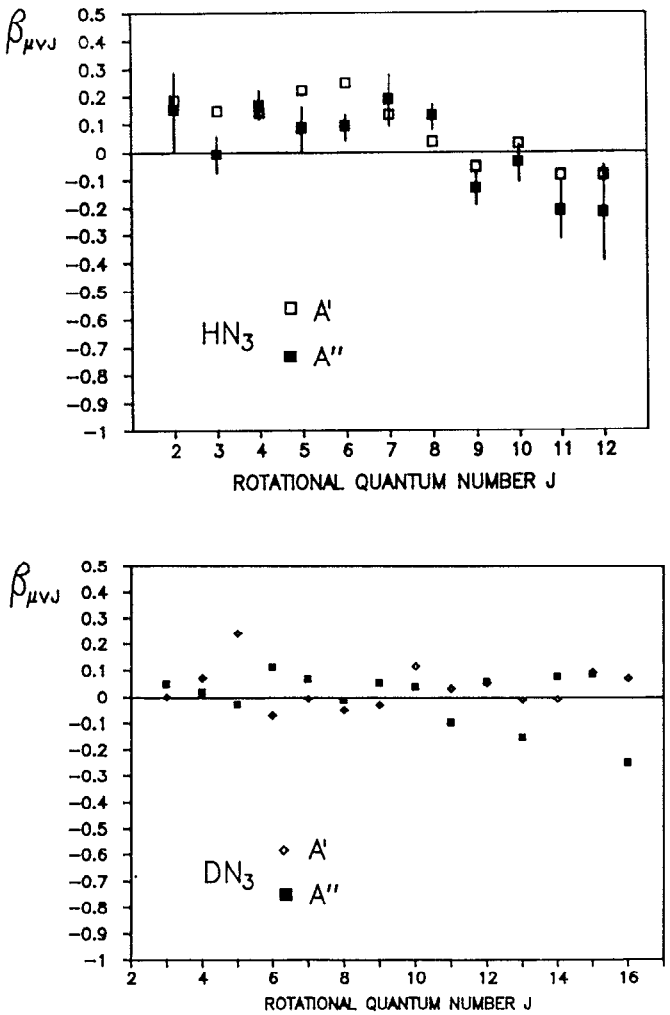

FIG. 7. Three-vector correlation $\langle \mu \cdot v \cdot J \rangle$ for NH (upper panel) and ND (lower panel) products. The Λ doublets are indicated by open squares, rhombi $^1\Delta(A')$, and solid squares, $^1\Delta(A'')$.

motion of the N_2-NR system due to conservation of angular momentum. However, the $\langle \mathbf{v} \cdot \mathbf{J} \rangle$ correlation for products generated in the $\Delta(A'')$ state is negative (only for the highest NH rotation β_{vJ} becomes slightly positive) and, thus, the upper potential-energy surface cannot induce a pure torsional motion of the NR rotor.

The value of the observed bipolar moment $\beta_{\mu vJ}$ which describes the three-vector correlation between $\boldsymbol{\mu}$ (R N_3), $\mathbf{v}$ (NR), and $\mathbf{J}$(NR) is close to zero (Fig. 7). If all three vectors are parallel to one another, then $\beta_{\mu vJ}$ will reach the limiting value of -1; if two vectors are parallel to one another, but the third one is perpendicular to these vectors, then $\beta_{\mu vJ}$ will reach the positive limit of $\beta_{\mu vJ} = +0.5$. A very weak tendency for $\beta_{\mu vJ}$ is observed for changing from positive values at low J to negative values at high J (Fig. 7). A significant difference between both Λ components is not observed. This is not astonishing because the three-vector correlation $\beta_{\mu vJ}$ is already weak and small differences between $\Delta(A')$ and $\Delta(A'')$ cannot be resolved.

IV. DISCUSSION

The applied spectroscopic technique based on line profile and polarization measurements provides a deep insight into the molecular motion in the course of fragmentation. All scalar properties which are summarized in Table II in conjunction with the measured vector correlations will be used in the following discussion of the dissociation process.

A. Transition dipole moment and dissociation time

Although the scalar and vector properties are integrated with respect to time, detailed information on the reaction path can be extracted, if only one potential energy surface is involved.[44]

The ground state of R N_3 is of $^1A'$ geometry and only the first electronically excited state $\tilde{A}\,^1A''$ can be reached at a photolysis wavelength of 308 nm.[46–48] The experimentally observed vertical excitation energy to the $\tilde{A}\,^1A''$ state of HN_3 is 4.68 eV (265 nm).[49] Thus, this state is reached at the long-wavelength end of absorption. Due to the isotopic shift, the excitation energy of DN_3 at 308 nm is "lower" compared to HN_3 (see E_a in Table II).

If the dissociation takes place in the R N_3 plane and if the parent molecule does not rotate, then the photoexcitation will strongly align the R N_3 in the lab frame and the ejected NR fragments must show a strong anisotropic spatial distribution, i.e., a strong $\langle \boldsymbol{\mu} \cdot \mathbf{v} \rangle$ correlation described by a $\beta_{\mu v}$ parameter at the theoretical limit of either $\beta_{\mu v}$ (min) $= -0.5$ or $\beta_{\mu v}$ (max) $= +1$. For a $^1A'' \leftarrow {}^1A'$ transition, the dipole moment $\boldsymbol{\mu}$ must be aligned perpendicular to the plane of symmetry of the parent. Thus one expects a value close to the theoretical limit of $\beta_{\mu v}$ (min) $= -0.5$ for the anisotropy parameter. A deviation from this limit is caused either by a change of the initial geometry or by rotation of the parent during fragmentation. We start with the model assumption that R N_3 becomes distorted in a plane. Then the $\langle \boldsymbol{\mu} \cdot \mathbf{v} \rangle$ correlation for a rotating R N_3 depends only on the time scale of the fragmentation, since $\boldsymbol{\mu}$ is aligned with $\mathbf{E}$, the electric field vector of the photolyzing laser beam at $t = 0$, but the recoil velocity $\mathbf{v}$ is determined at the moment

TABLE II. Scalar properties in the photodissociation of HN_3 and DN_3 at 308 nm.

	HN_3			DN_3		
	NH		N_2	ND		N_2
E_a/cm^{-1}		14 100		13 850		
E_{kin}/cm^{-1}	6950		3720	6430	3670	
E_{rot}/cm^{-1}	690		2740	1175		2580
f_{kin}	0.49		0.26	0.46		0.26
f_{rot}	0.05		0.20	0.08		0.19
$\langle v \rangle$/ms^{-1}	3310		1780	3100		1770
$\langle J \rangle$	5.5		37	10.5		36
$\Delta\nu_a$/cm^{-1}		0.135			0.14	
$\Delta\nu_i$/cm^{-1}		0.10			0.10	
$\Delta\nu_p$/cm^{-1}		0.058			0.057	
$\Delta\nu_f$/cm^{-1}		0.07			0.08	

of separation and is analyzed at times much longer than the lifetime of the excited complex: $\beta_{\mu v} = \langle P_2(\boldsymbol{\mu}_{t=0} \cdot \mathbf{v}_{t=\infty}) \rangle$. A deviation from the limiting value $\beta_{\mu v} = -0.5$ is attributed to (a) a deflection of the recoil velocity by the tangential velocity v_t of the rotating parent and (b) an R N_3 rotation by an angle $\delta = \omega \cdot \tau$ prior to fragmentation, where ω describes the angular velocity and τ the lifetime of the parent in the excited state.[50] Assuming a first-order decay reaction, an upper limit for the fragmentation time of DN_3 into DN and N_2 is given by $\tau \leqslant 120$ fs, where $\beta_{\mu v} = -0.4$ for the lowest DN rotational state is used in the calculations.[51] If we assume a molecular decay on an exponentially shaped potential-energy surface with respect to the distance of the ND and N_2 products, then the fragments are separated by 270 pm after that dissociation time.[44]

All important quantities of initial parent rotation which may influence the ejected products are summarized in Table III. The deflection angle $\theta \approx 5°$ is simply calculated from the observed mean recoil velocity $\langle v \rangle$ (see Table II) and the tangential velocity $v_t = \omega \cdot d$, where d is the distance from the center of mass of the parent to the center of mass of the product and $\omega = \sqrt{kT/\theta}$, with θ being the relevant moment of inertia. Obviously the recoil velocity is not significantly influenced by initial parent motion.

B. Origin of product rotation

The rotational excitation of the products is related to the torque provided by the gradient of the upper PES with respect to the three bending angles (see Table I). Fragment rotation may also be influenced by initial parent rotation about the three axes of inertia. In Table III the amount of transferred parent rotation to the product is given, with $kT/2$ for each degree of freedom. $\mathbf{J} \| \mathbf{v}$ is the projection of the rotational vector onto the recoil axis (for a planar fragmentation) and $\mathbf{J} \perp \mathbf{v}$ is the transferred rotation perpendicular to the recoil axis. The ND fragment picks up slightly more rotation from the parent than the NH product. However, in the dissociation processes of DN_3 and HN_3, much more product rotation is generated than transferred from initial parent motion (see Fig. 2) and, thus, parent motion may be neglected as a source of product rotation.

The Doppler profile measurements yield the internal energy of the partner fragment.[52,53] The photodissociation of HN_3 at shorter wavelengths generates N_2 fragments which are highly rotationally excited.[39,44,54] We assume that the substitution of hydrogen by deuterium will not strongly change the dissociation dynamics and, thus, the N_2 fragment will be formed with a considerable amount of rotation (see Table II). Although the transfer of initial parent rotation into the N_2 product is higher than into the NR product (see Table III), the extremely high N_2 product rotation is essentially caused by the dynamics on the upper PES.

Information about the N_2 rotational state distribution $P(J_{N_2})$ can be obtained from the wings of the Doppler lines.[44] We assume a Gaussian-like recoil velocity distribution of the fragments, where the width of the distribution $\Delta\nu_f$ is determined from the analyzed profile, $\Delta\nu_a$ [Eq. (2)]. $P(J_{N_2})$ can be extracted from the velocity distribution $f(v)$ of the NR fragment: $P(J) = f(v) \cdot (dv/dJ)$.[44] Figure 8 shows the N_2 product state distribution for NH and ND partner fragments. Both distributions are identical within the experimental accuracy. It should be mentioned that the analysis of the Doppler width was performed separately for both Λ sublevels, but no different behavior was observed. Thus, there is no correlation between the $\Delta(A')$ or $\Delta(A'')$ states and the N_2 rotation.

C. Electronic asymmetry and vector correlations

The most striking feature in the photodissociation dynamics of HN_3 and DN_3 at the long-wavelength end of the first electronic absorption spectrum is the different behavior of the Λ doublets in terms of the $\langle \boldsymbol{\mu} \cdot \mathbf{v} \rangle$ and $\langle \mathbf{v} \cdot \mathbf{J} \rangle$ correlation, while the population of both Λ sublevels is essentially the same (see Fig. 1).

A pure planar dissociation of R N_3 from the first electronic excited state $\tilde{A}\,^1A''$ should lead to NR fragments in the antisymmetric $^1\Delta(A'')$ state, because the wave function of the N_2 ($X\,^1\Sigma_g^+$) partner product is symmetric with respect to reflection at the fragmentation plane. In that case the vectors should also be aligned in a specific way: The recoil velocity $\mathbf{v}$ must be aligned perpendicular to the dipole moment $\boldsymbol{\mu}$; i.e., the anisotropy parameter $\beta_{\mu v}$ must be close to -0.5. The correlation between the translational and rotational motion of the fragment should also be strongly negative, because the rotational vector $\mathbf{J}$ is perpendicular to the plane of fragment rotation and, thus, perpendicular to the recoil direction. Table IV contains a summary of the observed vector correlations for low and high product rotation. The expected behavior of the vector correlations for a planar fragmentation is observed only for low J. Since the Doppler

TABLE III. Transfer of initial parent rotation, HN_3 and DN_3, onto the products, and upper limit for the dissociation time τ.

	NH	N_2	ND	N_2
v_t/ms^{-1}	288	154	275	157
$\omega/10^{12}$ s^{-1}	2.41		2.33	
$\alpha = tg^{-1}(v_t/\langle v \rangle)$	5.0°		5.1°	
τ/fs	160		120	
$J \| v/\hbar$	2.2	0.1	3.0	0.2
$J \perp v/\hbar$	0.4	4.8	0.7	4.7

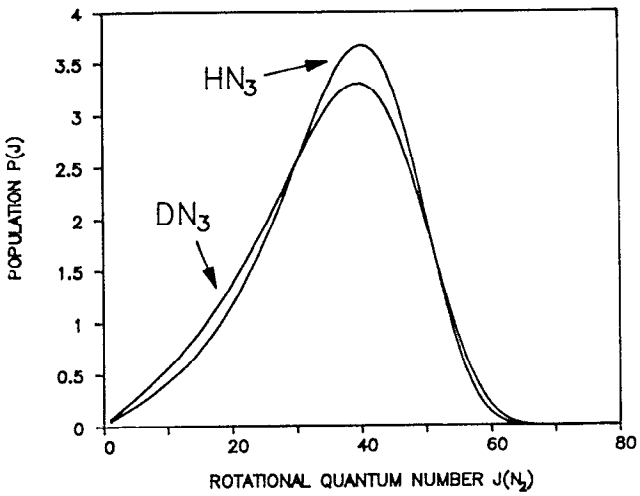

FIG. 8. Rotational state distribution $P(J_{N_2})$ of the N_2 partner product formed in the photodissociation of $R\,N_3$ at 308 nm. $P(J_{N_2})$ is obtained by line-profile analysis of the NR product.

width is essentially independent of J_{ND}, the N_2 partner products of ND fragments in low rotational states are generated with a significant amount of rotation. This N_2 rotation must be caused by an in-plane bending motion. The conservation of total angular momentum $\mathbf{J}_t$ is fulfilled by the orbital angular momentum $\mathbf{l}$ of the ND-N_2 system, $\mathbf{J}_t = \mathbf{J}_{ND} + \mathbf{J}_{N_2} + \mathbf{l}_{ND\text{-}N_2}$. For high ND product rotation, the DN_3 system behaves differently and the importance of nonplanar geometries in the excited state dissociation dynamics is evident.

In the ground-state dissociation of HN_3 ($\tilde{X}\,^1A'$), following overtone excitation, King and co-workers[43] observed a preferred population of the symmetric NH $\Delta(A')$ state, as expected for a planar dissociation. Alexander *et al.*[41] developed a model to predict this Λ doublet preference. In that Franck–Condon model, the electronic-vibrational wave function, Ψ_i, of the N_2-NH system at the transition state (determined by *ab initio* calculations[55]) is projected onto the electronic-rotational wave function of the free NH rotor, Ψ_f:

$$P(J,M,\Lambda) = |\langle \Psi_f | \Psi_i \rangle|^2. \tag{9}$$

TABLE IV. Vector correlations in the photodissociation of HN_3 and DN_3 at 308 nm. The influence of the electronic asymmetry in NH ($^1\Delta$) state Λ doublets on the dissociation dynamics is documented by the different β values for NR fragments generated either in the $^1\Delta(A')$ or in the $^1\Delta(A'')$ state. The fraction of fragment rotation which is generated by a torsional motion of the NR rotamer is given by $f_{torsion}$.

	Low J			High J		
	$\beta_{\mu v}$	$\beta_{\omega J}$	$f_{torsion}$	$\beta_{\mu v}$	$\beta_{\omega J}$	$f_{torsion}$
NH(A')	−0.31	−0.1	0.27	+0.05	+0.25	0.50
(A'')	−0.35	−0.20	0.20	−0.04	+0.05	0.37
ND(A')	−0.40	−0.20	0.20	+0.20	+0.20	0.47
(A'')	−0.40	−0.20	0.20	−0.10	−0.20	0.20

The calculated ratio

$$R(J) = \frac{P(J,A')}{P(J,A'')} = \sum_M P(J,M,A') / \sum_M P(J,M,A'') \tag{10}$$

agrees well with the one determined in the experiment.[43]

The vector correlation between the recoil velocity $\mathbf{v}$ and the rotational vector $\mathbf{J}$ was also calculated assuming that the NH fragment is ejected along the N_3 chain. The predicted value of the corresponding β_{vJ} parameter was significantly smaller [β_{vJ}(theory) $= -0.39$] than the experimentally measured value [β_{vJ}(experiment) $= 0.17 \pm 0.06$]. Probably the dissociation geometry in the exit channel changes in such a way that the NH angular momentum is more strongly induced by a torsional motion of the parent. This out-of-plane motion leads to a NH motion like a propeller driven airplane, i.e., a preferred parellel alignment between $\mathbf{v}$ and $\mathbf{J}$.

Out-of-plane motions are very important in the $R\,N_3$ UV dissociation at 308 nm discussed in the present paper. Thus, the simple Franck–Condon-type model cannot be adopted to predict the different behavior of the Λ doublets. In the following we first want to consider the charge density of the Λ doublets.

The non-normalized wave function of the two π electrons which form the electronic states in NR are given by

$$a\,^1\Delta(A') \equiv \cos(\varphi_1 + \varphi_2), \tag{11a}$$

$$a\,^1\Delta(A'') \equiv \sin(\varphi_1 + \varphi_2), \tag{11b}$$

$$b\,^1\Sigma^+ \equiv \cos(\varphi_1 - \varphi_2), \tag{11c}$$

$$X\,^3\Sigma^- \equiv \sin(\varphi_1 - \varphi_2). \tag{11d}$$

The angles φ_i measure the angles from electron 1 and electron 2 to an axis perpendicular to the NR bond. In Fig. 7 of Ref. 39 the lobe of a single Δ electron is shown to illustrate its spatial distribution. If we combine two π electrons to a Δ state, then the charge density $\rho(\varphi)$ is given by

$$\rho(\varphi) \sim \int_0^{2\pi} \psi(\varphi_1,\varphi_2)\psi^*(\varphi_1,\varphi_2)\,d\varphi_2 = \int_0^{2\pi} \psi(\varphi_1,\varphi_2)\psi^*(\varphi_1,\varphi_2)\,d\varphi_1, \tag{12}$$

$$\rho(\varphi = \varphi_1)_{A'} \sim \int_0^{2\pi} \cos^2(\varphi_1 + \varphi_2)\,d\varphi_2 = \text{const}, \tag{13}$$

$$\rho(\varphi = \varphi_2)_{A''} \sim \int_0^{2\pi} \sin^2(\varphi_1 + \varphi_2)\,d\varphi_2 = \text{const}. \tag{14}$$

Thus, the charge density has cylindrical symmetry, i.e., it is independent of φ and identical for both Λ sublevels: $\rho(\varphi)_{A'} = \rho(\varphi)_{A''}$. The probability density of observing electron 1 at the same position as electron 2, i.e., $\varphi_1 = \varphi_2 = \varphi$, is given by

$$|\psi(\varphi_1)_{A'}|^2 \sim \cos^2(2\varphi), \tag{15a}$$

$$|\psi(\varphi_2)_{A''}|^2 \sim \sin^2(2\varphi), \tag{15b}$$

which corresponds to the typical "four-leafed-clover"-shape of a Δ electron.

It is important to note that the vector correlations are not necessarily identical for the $\Delta(A')$ and the $\Delta(A'')$ state. For example, the $\langle \mathbf{v}\cdot\mathbf{J} \rangle$ correlation described by the β_{vJ} pa-

rameter is the second moment of the M distribution of the rotation about the recoil axis. For a given NR level (J,Λ), where Λ represents, in an unconventional way, the $\Delta(A')$ or $\Delta(A'')$ level, the correlation between the translational and rotational motion of the fragment is given by

$$\beta_{vJ}(J,\Lambda) = \sum_M \frac{3M^2 - J(J+1)}{2J(J+1)} P(J,M,\Lambda) \Big/ \sum_M P(J,M,\Lambda). \tag{16}$$

If only the magnetic sublevel $M=0$ is populated, $P(J,M\neq 0,\Lambda)=0$, then the value of the parameter β_{vJ} is -0.5. On the other hand, if only the levels $M=J$ and $M=-J$ are populated, then

$$\beta_{vJ}(J,\Lambda) = 1 - \frac{3}{2J+2}, \tag{17}$$

and in the high J limit, we obtain $\beta_{vJ}(J\rightarrow\infty,\Lambda) = +1$. As an example, we contemplate the $J=2$ state where only the $M=0$ sublevel of the $\Delta(A'')$ state is populated, while for the symmetric $\Delta(A')$ state the $M=\pm 2$ levels are populated. Then we obtain $\beta_{vJ}(J=2,A'') = -0.5$ and $\beta_{vJ}(J=2,A') = +0.5$, although the populations $P(J=2,A')$ and $P(J=2,A'')$ are the same.

In the present experiment the difference $\Delta P(J)$ between the populations of the Λ levels vanishes,

$$\Delta P(J) = P(J,A') - P(J,A'')$$

$$= \sum_M [P(J,M,A') - P(J,M,A'')] = 0, \tag{18}$$

and the difference between the $\beta_{vJ}(J,\Lambda)$ parameters for the A' and A'' states is given by

$$\Delta\beta_{vJ}(J) = \beta_{vJ}(J,A') - \beta_{vJ}(J,A'')$$

$$= \frac{3}{2J(J+1)} \sum_M M^2 [P(J,M,A') - P(J,M,A'')] \Big/ \sum_M P(J,M,\Lambda). \tag{19}$$

We observe an increasing positive value of $\Delta\beta_{vJ}(J)$ for increasing J, indicating the preferred population of high $|M|$ levels in the $^1\Delta(A')$ state relative to those of the $^1\Delta(A'')$ state. We simply assume a square dependence of the population of the magnetic sublevels, such that $P(J,M,A')$ increases with increasing $P(J,M,A') \sim a(A')J^2 + M^2$, while $P(J,M,A'')$ decreases, $P(J,M,A'') \sim a(A'')J^2 - M^2$. In the high J limit we observe for the ND fragment $\beta_{vJ}(A') = +0.2$ and $\beta_{vJ}(A'') = -0.2$ (see Table IV). These values will be reproduced for $a(A') = \frac{1}{3}$ and $a(A'') = 1$. The corresponding $P(M)$ distributions are shown in Fig. 9.

The spatial distribution of the ND fragments is also different for both Λ components (see Table IV). While ND products generated in the antisymmetric $^1\Delta(A'')$ state are preferentially ejected in the plane of the parent, i.e. perpendicular to the axis of the transition dipole moment μ, the recoil of the ND(A') fragments is more parallel to μ. Thus, especially for these fragments, DN_3 is distorted by a NN-ND out-of-plane bend configuration. However, the ND(A'') products must also have moved away from the initial plane, because the $\beta_{\mu v}$ parameter increased from $\beta_{\mu v}(A'', \text{low } J) = -0.4$ to $\beta_{\mu v}(A'', \text{high } J) = -0.1$. We can calculate an average angle $\theta_{\mu v}$ between μ and the final recoil direction: $\beta_{\mu v} = \langle P_2(\cos\theta_{\mu v})\rangle$. For ND$(A'', \text{high } J)$ we obtain $\theta_{\mu v}(A'') \simeq 59°$ and for the fragments generated in the symmetric Λ level $\theta_{\mu v}(A') \simeq 47°$, where an instantaneous dissociation has been assumed. These angles will slightly change to $\theta_{\mu v}(A'') \simeq 60°$ and $\theta_{\mu v}(A') \simeq 45°$, if we consider a time of fragmentation calculated from low J values. The spatial distribution of the ND(A'') and ND(A') products is shown in Fig. 10.

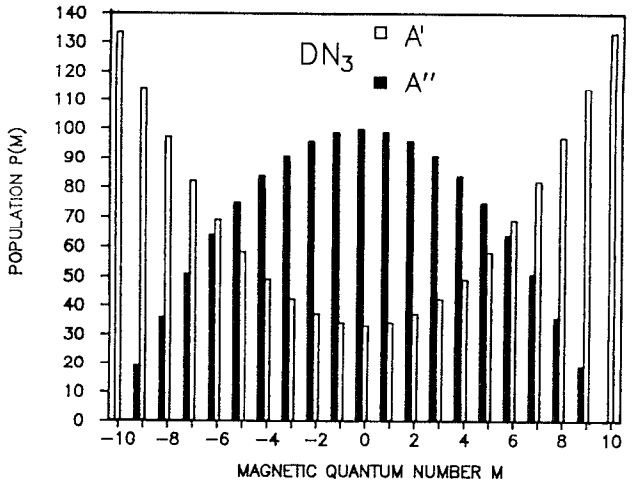

FIG. 9. ND population distribution $P(M)$ of the magnetic sublevels in the photodissociation of DN_3 at 308 nm. The Λ components $^1\Delta(A')$, open bars, and $^1\Delta(A'')$, solid bars, show different behavior.

The different behavior of the Λ components in terms of the vector correlations has not been observed in the dissocia-

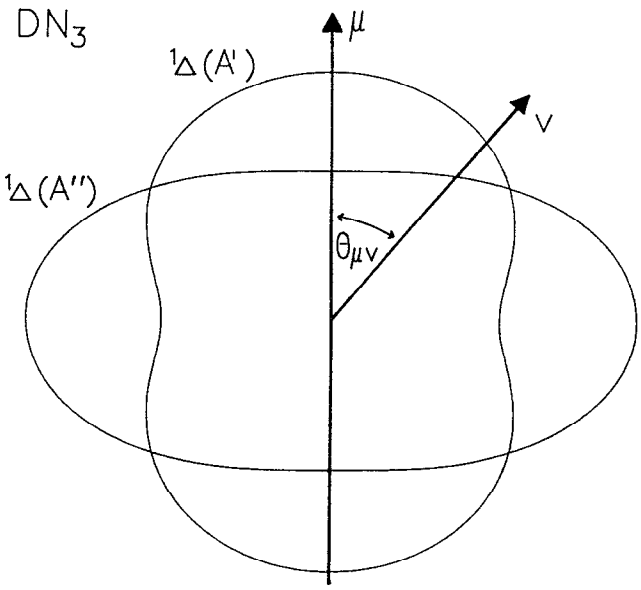

FIG. 10. Spatial distribution of ND products in high-rotational states generated in the $^1\Delta(A')$ or in the $^1\Delta(A'')$ state.

tion of HN_3 at higher excitation energies (248 nm, 266 nm) which are close to the absorption maximum, $\lambda(\sigma_{max}) = 265$ nm.[39,40,44] A careful check of our former measurements shows that at 248 nm, both Λ doublets behave identically. At 266 nm, a very small difference in the line profiles at high J is barely observable. At 308 nm, the vector correlations of $NH(A')$ and $NH(A'')$ are different and this difference becomes even more pronounced in the photofragmentation of DN_3 which needs slightly higher excitation energies ($\Delta E \simeq 250\ cm^{-1}$, see Table II). At the long-wavelength end of the absorption spectrum, regions of the upper PES different from the equilibrium geometry are probed. Since the potential energy of the molecule on the upper PES decreases at larger NN-NR distances for a bent NN-NR configuration, it is expected that the different behavior of the Λ components originates from motions at those dissociation geometries.

V. CONCLUSION

The experimentally observed scalar and vector properties of HN_3 and DN_3 fragmentation at 308 nm can be explained by a dissociation process, where product rotation is composed of breaking parent bending (in-plane and out-of-plane) vibrations and of an angular dependence of the $\tilde{A}\,^1A''$ state. The weighting of the single factors is different in HN_3 and DN_3 and specific for each rotational state. The bipolar moments $\beta_{\mu J}$, $\beta_{\mu v}$, and β_{vJ} are direct representations of the contributing effects, since these result in different vector correlations. Assuming that the transition state in the $R\,N_3$ photodissociation is roughly planar, fragment rotation due to breaking of parent in-plane bending modes will align $\boldsymbol{\mu} \| \mathbf{J}$ and $\mathbf{v} \perp \mathbf{J}$, whereas N_2–NR bond cleavage by torsional excitation will lead to $\boldsymbol{\mu} \perp \mathbf{J}$ and $\mathbf{v} \| \mathbf{J}$. Therefore, high NR rotation originates predominantly from the internal torsional motion of $R\,N_3$, and that mainly from the torque provided by the angular dependence of the $\tilde{A}\,^1A''$ state. For low J, in-plane bending motion is essential for the fragmentation process which is turned out by the strong negative $\langle \boldsymbol{\mu} \cdot \mathbf{v} \rangle$ and $\langle \mathbf{v} \cdot \mathbf{J} \rangle$ vector correlations.

Despite the observation of a pronounced difference in product internal energy disposal at the 308 nm fragmentation of the isotopic hydrazoic acid (see Table II), it is likely to explain the process by a uniform mechanism, which is determined by the nearly identical potential surfaces. The higher rotational excitation in ND seems to be due to the much longer ND lever arm being about 12.5% of the N—D distance and, hence, almost twice as long as that of NH.

The origin of NR rotation is an in-plane bending motion of the NNN chain leading to a negative β_{vJ} parameter and an out-of-plane motion which results in a positive value for β_{vJ}. Due to the larger mass of the D atom one rather expects a stronger motion in the original plane of the parent resulting in a more pronounced negative $\langle \mathbf{v} \cdot \mathbf{v} \rangle$ and $\langle \mathbf{v} \cdot \mathbf{J} \rangle$ correlation which is observed in the experiment.

The most striking result in the fragmentation of $R\,N_3$ at 308 nm is the influence of the electronic asymmetry in $NR(^1\Delta)$ Λ doublets on the photodissociation dynamics. While the population of the Λ sublevels is the same within a few percent, the vector correlations are significantly different. NR products in the asymmetric $^1\Delta(A'')$ state are generated with a preferred perpendicular alignment between $\boldsymbol{\mu}$, the transition dipole moment of the parent, and $\mathbf{v}$, the recoil velocity of the product. This is expected for a planar dissociation process where the dipole moment $\boldsymbol{\mu}$ of the $\tilde{A}\,^1A'' \leftarrow \tilde{X}\,^1A'$ transition is perpendicular to the molecular plane. The rotational vector $\mathbf{J}$ is preferentially aligned perpendicular to the propagation direction of the product and the rotation is essentially caused by an in-plane bending motion of the N_3 chain. NR products in the symmetric $^1\Delta(A')$ state are formed at high J with a preferred parallel alignment between $\boldsymbol{\mu}$ and $\mathbf{v}$ indicating the importance of nonplanar geometries in the excited-state dissociation dynamics.

The nonplanarity of the process for generating NR products in the $^1\Delta(A')$ state is also evident from the $\langle \mathbf{v} \cdot \mathbf{J} \rangle$ correlation. At high fragment rotation the translational and rotational vectors are aligned preferentially parallel to one another which corresponds to a torsional motion of the NR (A') rotor. In order to explain these Λ doublet propensities, which were observed for the first time, a model has to deal explicitly with the two-electron character of the $^1\Delta$ state.

ACKNOWLEDGMENTS

Support of this work by the Deutsche Forschungsgemeinschaft is gratefully acknowledged. We thank Professor E. A. Reinsch for fruitful discussions and his support in the analysis of the Λ doublet wave functions.

[1] R. N. Dixon, J. Chem. Phys. **85**, 1866 (1986).
[2] K.-H. Gericke, S. Klee, F. J. Comes, and R. N. Dixon, J. Chem. Phys. **85**, 4463 (1986).
[3] *Molecular Photodissociation Dynamics*, edited by M. N. R. Ashfold and J. E. Baggott (The Royal Society of Chemistry, London, 1987).
[4] M. P. Docker, Chem. Phys. **135**, 405 (1989).
[5] M. H. Alexander *et al.*, J. Chem. Phys. **89**, 1749 (1988).
[6] M. H. Alexander and P. J. Dagdigian, J. Chem. Phys. **80**, 4325 (1985).
[7] B. Pouilly, P. J. Dagdigian, and M. H. Alexander, J. Chem. Phys. **87**, 7118 (1987).
[8] P. Andresen and E. W. Rothe, J. Chem. Phys. **82**, 3634 (1985).
[9] M. J. Bronikowski and R. N. Zare, Chem. Phys. Lett. **166**, 5 (1990).
[10] Ch. Ottinger, R. Velasco, and R. N. Zare, J. Chem. Phys. **52**, 1636 (1970).
[11] K. Bergmann and W. Demtröder, J. Phys. B **5**, 1386 (1972).
[12] Ch. Ottinger, Chem. Phys. **1**, 161 (1973).
[13] R. P. Mariella, Jr. and A. C. Luntz, Jr., J. Chem. Phys. **67**, 5388 (1977).
[14] R. P. Mariella, Jr., B. Lantzsch, V. T. Maxon, and A. C. Luntz, Jr., J. Chem. Phys. **69**, 5411 (1978).
[15] K.-H. Gericke, G. Ortgies, and F. J. Comes, Chem. Phys. Lett. **69**, 156 (1980).
[16] E. J. Murphy, J. H. Brophy, G. S. Arnold, W. L. Dimpfl, and J. L. Kinsey, J. Chem. Phys. **74**, 324 (1981).
[17] J. E. Butler, G. M. Jursich, I. A. Watson, and J. R. Wiesenfeld, J. Chem. Phys. **84**, 5365 (1986); C. B. Cleveland, G. M. Jurisch, M. Trolier, and J. R. Wiesenfeld, J. Chem. Phys. **86**, 3253 (1987); C. R. Park and J. R. Wiesenfeld, Chem. Phys. Lett. **163**, 230 (1989).
[18] W. E. Hollingsworth, J. Subbiah, G. W. Flynn, and R. E. Westson, Jr., J. Chem. Phys. **82**, 2295 (1985).
[19] K. G. McKendrick, D. J. Rakestraw, and R. N. Zare, Faraday Discuss. Chem. Soc. **84**, 39 (1987); M. J. Bronikowski, R. Zhang, D. J. Rakestraw, and R. N. Zare, Chem. Phys. Lett. **156**, 7 (1989).
[20] K. Kleinermanns, E. Linnebach, and M. Pohl, J. Chem. Phys. **91**, 2181 (1989).
[21] A. M. L. Irvine, I. W. M. Smith, R. P. Tuckett, and X-F. Yang, J. Chem. Phys. **93**, 3177 (1990).

[22] D. G. Sauder and P. J. Dagdigian, J. Chem. Phys. **92**, 2389 (1990).
[23] A. M. Irvine, I. W. M. Smith, and R. P. Tuckett, J. Chem. Phys. **93**, 3187 (1990).
[24] J. Derouard, T. N. Nguyen, and N. Sadeghi, J. Chem. Phys. **72**, 6698 (1980).
[25] H. Helm, P. C. Cosby, M. M. Graff, and J. T. Mosely, Phys. Rev. A **25**, 304 (1982).
[26] R. Vasudev, R. N. Zare, and R. N. Dixon, J. Chem. Phys. **80**, 4863 (1984).
[27] P. Andresen, G. S. Ondrey, B. Titze, and E. W. Rothe, J. Chem. Phys. **80**, 2548 (1984); D. Häusler, P. Andresen, and R. Schinke, J. Chem. Phys. **87**, 3949 (1987).
[28] A. U. Grunewald, K.-H. Gericke, and F. J. Comes, J. Chem. Phys. **87**, 5709 (1987); **89**, 345 (1988).
[29] M. P. Docker, A. Hodgson, and J. P. Simons, Faraday Discuss. Chem. Soc. **82**, 25 (1986); M. Brouard, M. T. Martinez, J. O'Mahony, and J. P. Simons, J. Chem. Soc. Faraday Trans. 2 **85**, 1207 (1989); Mol. Phys. **69**, 65 (1990).
[30] G. Radhakrishnan, S. Buelow, and C. Wittig, J. Chem. Phys. **84**, 727 (1986); S. Buelow, G. Radhakrishnan, and C. Wittig, J. Phys. Chem. **91**, 5409 (1987); D. Häusler, J. Rice, and C. Wittig, *ibid.* **91**, 5413 (1987).
[31] C. X. W. Qian, A. Ogai, L. Iwata, and H. Reisler, J. Chem. Phys. **89**, 6547 (1988); Y. Y. Bai, A. Ogai, C. X. W. Qian, L. Iwata, G. A. Segal, and H. Reisler, *ibid.* **90**, 3903 (1989); C. X. W. Qian, A. Ogai, L. Iwata, and H. Reisler, *ibid.* **92**, 4296 (1990).
[32] J. H. Shan and R. Vasudev, Chem. Phys. Lett. **141**, 472 (1987); J. H. Shan, V. Vorsa, S. J. Wategaonkar, and R. Vasudev, J. Chem. Phys. **90**, 5493 (1989).
[33] A. Sinha, R. L. Vander Wal, and F. F. Crim, J. Chem. Phys. **91**, 2929 (1989).
[34] M. Dubs, U. Brühlmann, and J. R. Huber, J. Chem. Phys. **84**, 3106 (1986); A. E. Bruno, U. Brühlmann, and J. R. Huber, Chem. Phys. Lett. **120**, 155 (1988); U. Brühlmann and J. R. Huber, *ibid.* **143**, 199 (1988).
[35] F. Lahmani, C. Lardeux, and D. Solgadi, Chem. Phys. Lett. **129**, 24 (1986).
[36] R. Lavi, I. Bar, and S. Rosenwaks, J. Chem. Phys. **86**, 1639 (1987); R. Lavi, D. Schwartz-Lavi, I. Bar, and S. Rosenwaks, J. Phys. Chem. **91**, 5398 (1987).
[37] F. Alberti and A. E. Douglas, Chem. Phys. **34**, 399 (1978).
[38] A. M. Quinton and J. P. Simons, Chem. Phys. Lett. **81**, 214 (1984); J. P. Simons, J. Phys. Chem. **91**, 5378 (1987).
[39] K.-H. Gericke, R. Theinl, and F. J. Comes, J. Chem. Phys. **92**, 6548 (1990).
[40] K.-H. Gericke, R. Theinl, and F. J. Comes, Chem. Phys. Lett. **164**, 605 (1990).
[41] M. H. Alexander, P. J. Dagdigian, and H.-J. Werner, Faraday Discuss. Chem. Soc. **91** (1991).
[42] J. C. Stephenson, M. P. Casassa, and D. S. King, J. Chem. Phys. **89**, 1378 (1988).
[43] B. R. Foy, M. P. Casassa, J. C. Stephenson, and D. S. King, J. Chem. Phys. **89**, 608 (1988); **90**, 7037 (1989); **92**, 2782 (1990); M. P. Casassa, B. R. Foy, J. C. Stephenson, and D. S. King, *ibid.* **94**, 250 (1991).
[44] K.-H. Gericke, T. Haas, M. Lock, R. Theinl, and F. J. Comes, J. Phys. Chem. **95**, 6104 (1991).
[45] K.-H. Gericke, Faraday Discuss. Chem. Soc. **91** (1991).
[46] U. Meier, Dissertation, Fakultät für Chemie, Ruhr-Universität Bochum, 1988.
[47] U. Meier and V. Staemmler (unpublished).
[48] U. Meier and V. Staemmler, J. Phys. Chem. **95**, 6111 (1991).
[49] J. R. McDonald, J. W. Rabalais, and S. P. McGlynn, J. Chem. Phys. **52**, 1332 (1970).
[50] G. E. Busch and K. R. Wilson, J. Chem. Phys. **56**, 3638 (1972); **56**, 3655 (1972).
[51] C. Jonah, J. Chem. Phys. **55**, 1915 (1971).
[52] K.-H. Gericke, Phys. Rev. Lett. **60**, 561 (1988).
[53] K.-H. Gericke, H. G. Gläser, C. Maul, and F. J. Comes, J. Chem. Phys. **92**, 415 (1990).
[54] J.-J. Chu, P. Marcus, and P. J. Dagdigian, J. Chem. Phys. **93**, 257 (1990).
[55] M. H. Alexander, T. Hemmer, H.-J. Werner, and P. J. Knowles, J. Chem. Phys. **93**, 3307 (1990).
[56] J. Pendtsen, F. Hegelund, and F. M. Nicolaisen, J. Mol. Spectros. **128**, 309 (1988); D. M. Levine and D. A. Dows, J. Chem. Phys. **46**, 1168 (1967).